



Enhanced electrocatalytic oxidation of formic acid by platinum deposition on ruthenium nanoparticle surfaces

Wei Chen, Li-Ping Xu, Shaowei Chen *

Department of Chemistry and Biochemistry, University of California, 1156 High Street, Santa Cruz, CA 95064, United States

ARTICLE INFO

Article history:

Received 30 September 2008

Received in revised form 11 March 2009

Accepted 17 March 2009

Available online 25 March 2009

Keywords:

Formic acid

Electro-oxidation

PtRu

STM

Electrochemical impedance

ABSTRACT

PtRu alloy nanoparticles were prepared by the spontaneous adsorption of $\text{Pt}(\text{acac})_2$ on the surface of freshly prepared octanethiolate-protected ruthenium (RuSC8) nanoparticles. UV–vis spectroscopic measurements suggested that the adsorption was facilitated by the strong affinity of the platinum metal center to the ruthenium surface. Scanning tunneling spectroscopic studies showed that the resulting PtRu nanoparticles exhibited enhanced conductance as compared to the original ruthenium nanoparticles, where the adsorbed Pt centers might serve as the effective sites for electron-tunneling across the tip/particle/substrate junction. The nanoparticles were then loaded onto a glassy carbon (GC) electrode and their catalytic activities in the electro-oxidation of formic acid were examined and compared. Remarkably, despite the presence of an organic protecting monolayer on the particle surface, apparent electrocatalytic activity was observed. Voltammetric measurements suggested that a Pt skin layer was formed on the Ru nanoparticle surface, most likely as a result of electro-reduction of the adsorbed $\text{Pt}(\text{acac})_2$. On the basis of the onset potential and current density in the electro-oxidation of HCOOH , the resulting PtRu nanoparticles displayed much higher electrocatalytic activity than the Ru counterparts and commercial PtRu nanoparticle catalysts from BASF. It was also found that the electrocatalytic activity of the PtRu nanoparticles was comparable to that of FePt alloy nanoparticles and PtRu bulk electrocatalysts, despite a minimal loading of Pt in the catalysts. Consistent responses were observed in electrochemical impedance spectroscopic measurements, where the charge-transfer resistance on PtRu/GC was found to be at least an order of magnitude smaller than that on Ru/GC and commercial PtRu catalysts. These measurements suggest that the PtRu thin-layer nanoparticles might be used as a promising candidate for the electrocatalytic oxidation of formic acid.

© 2009 Elsevier B.V. All rights reserved.

1. Introduction

Fuel cells are electrochemical devices which convert chemical energy directly to electrical energy with high conversion efficiency and low environmental pollution. In recent years, numerous studies have been focused on direct methanol fuel cells (DMFC) and direct formic acid fuel cells (DFAFC) [1–8]. However, despite substantial progress, a number of challenges remain. One of these is the slow electro-oxidation kinetics of fuels on anode catalysts that reduces the energy conversion efficiency. This is mainly caused by the poisonous intermediates (primarily CO) that are irreversibly adsorbed on the catalyst surface and the resulting impeded accessibility of the catalytic sites by fuel molecules. In order to minimize the self-poisoning of catalysts, various Pt-based alloys have been prepared and evaluated in the electrocatalytic oxidation of methanol or formic acid [9–20]. Among these, PtRu alloys exhibit the highest catalytic activity. This is mainly accounted for by the

dual-pathway mechanism (direct and indirect paths), which has been widely accepted in the interpretation of the electro-oxidation of organic fuels such as methanol and formic acid. In the indirect path, the formation of an oxygen-containing surface on the second metal facilitates the oxidative removal of poisoning intermediates (e.g., CO) that are adsorbed on the Pt sites. For instance, it has been found that a less positive electrode potential is required for the dissociation of water and the formation of OH species on ruthenium than on platinum surfaces [21–23], where the resulting Ru–OH species act as a source of atomic oxygen for the oxidation of adsorbed CO to CO_2 .

Various synthetic strategies have been reported in the preparation of PtRu alloy electrocatalysts, such as spontaneous deposition [24], coimpregnation method [25–27], colloidal synthesis [28,29], microwave irradiation [30–32], electrodeposition [33–35], and microemulsions [36]. In these, one key goal is to minimize the loading of precious metals and hence lower the costs of the catalysts, but without compromising the catalytic performance. Recently, near-surface-alloy (NSA) structures have attracted much attention in the study of fuel cell electrocatalysis [37–39]. In NSA

* Corresponding author.

E-mail address: schen@chemistry.ucsc.edu (S. Chen).

catalysts, only a monolayer or sub-monolayer of precious transition metals is deposited onto a host metal surface. Largely because of the formation of surface metal–metal bonds, the catalytic activity of NSA may be drastically improved as compared to that of the individual metal components [40]. For instance, Arenz et al. [41] studied methanol and formic acid oxidation on Pt(111) modified by a pseudomorphic Pd monolayer formed by electrochemical deposition. It was found that the single layer of Pd on Pt(111) was about four times more active than the original Pt surface for HCOOH oxidation, because of the direct HCOOH oxidation path (no CO poisoning) on the Pd monolayer. Recently, Wieckowski and coworkers [42] and Adzic et al. [43,44] prepared PtRu nanoparticles by the spontaneous deposition of Pt (sub)monolayers on Ru particle surfaces and studied their catalytic properties as fuel cell anodes. All the samples showed higher electrocatalytic activities and better CO tolerance than the original Ru particles. These studies suggest that the NSA nanoparticles may be used as ideal electrocatalysts for fuel cells with high activity and minimal Pt loading.

In this report, a new route was presented for the platinum functionalization of ruthenium nanoparticles, and formic acid oxidation was used as a yardstick to measure their electrocatalytic activity. Experimentally, ruthenium nanoparticles protected by 1-octanethiol were firstly prepared. Spontaneous adsorption of Pt(acac)₂ onto the nanoparticles was initiated when the particles were mixed with Pt(acac)₂, despite the surface protecting layer. A platinum skin layer was then formed on the Ru nanoparticle surface by electrochemical reduction. The resulting nanoparticles were deposited onto a glassy carbon (GC) electrode surface (denoted as Ru/GC and PtRu/GC electrodes, respectively) and the electrochemical performance in formic acid oxidation was then examined and compared by voltammetric and electrochemical impedance measurements. The results showed that despite the presence of an organic protecting shell, the particles exhibited apparent electrocatalytic activity in formic acid oxidation, which was improved significantly by the deposition of a thin surface layer of Pt. Comparative studies were also carried out with commercial PtRu/C catalysts.

2. Experimental

2.1. Materials

Ruthenium chloride (RuCl₃, 99%, ACROS), Pt(acetylacetonate)₂ (Pt(acac)₂, 99%, ACROS), 1,2-propanediol (ACROS), sodium acetate trihydrate (NaAc · 3H₂O, MC&B), 1-octanethiol (C8SH, 96%, ACROS), perchloric acid (HClO₄, 99.999%, Fisher), and formic acid (HCOOH, 99%, ACROS) were used as received. Water was supplied by a Barnstead Nanopure water system (18.3 MΩ cm). Commercial catalysts of 10 wt% PtRu alloys (atomic ratio 1:1) supported on Vulcan XC-72 were obtained from BASF Fuel Cell Inc.

2.2. Nanoparticle preparation

Ruthenium nanoparticles were synthesized by thermolytic reduction of ruthenium chloride in 1,2-propanediol according to the procedure described previously [45–47]. Briefly, 0.65 mmol of RuCl₃ and 2 mmol of NaAc were dissolved in 200 mL of 1,2-propanediol. The mixed solution was heated to 165 °C for 15 min under vigorous stirring. During the reaction, the color of the solution was found to change from red to pale green and finally to dark brown indicating the formation of Ru nanoparticles. After the colloid solution cooled to room temperature, a calculated amount of C8SH in toluene was added into the solution under magnetic stirring. Intense color appearance was observed in the toluene phase whereas the diol phase became colorless, signifying the extraction

of the particles from the diol phase to the toluene phase. With the addition of 20 mL of Nanopure water to further separate the two phases, the toluene portion was collected and dried at reduced pressure. Copious methanol was then used to remove excessive ligands, affording purified Ru nanoparticles which were denoted as RuSC8. The resulting RuSC8 nanoparticles were found to be soluble in apolar solvents, such as dichloromethane, hexane, but not in polar solvent such as alcohols and water. The core diameter of the Ru particles was found to be 2.12 ± 0.72 nm as determined by transmission electron microscopy (TEM) measurements [47].

Spontaneous adsorption of platinum on the ruthenium nanoparticle surface was carried out with freshly prepared RuSC8 nanoparticles. In a typical reaction, 1 mL of 0.1 mM Pt(acac)₂ in dichloromethane was added into 2 mL of 1 mg/mL RuSC8 particles in dichloromethane. The mixed solution was then stirred overnight under a N₂ atmosphere. After the reaction, acetone was used to wash the Pt decorated Ru nanoparticles several times to remove excessive Pt(acac)₂. UV–vis spectroscopic studies of the nanoparticles as well as the acetone supernatants were performed with an ATI Unicam UV4 spectrometer using a 1-cm quartz cuvette with a resolution of 2 nm. The resulting particles were denoted as PtRu.

2.3. Electrochemistry

Prior to the deposition of the Ru and PtRu nanoparticles onto an electrode surface for electrocatalytic assessment, a glassy carbon (GC) electrode (Bioanalytical Systems and 3.0 mm diameter) was polished with alumina slurries (0.05 μm) and cleansed by sonication in 0.1 M HNO₃, H₂SO₄ and Nanopure water for 10 min successively. 10 μL of Ru, and PtRu nanoparticles dissolved in dichloromethane and commercial PtRu nanoparticles dispersed in Nafion (H₂O/Nafion volume ratio 70:30) (all at 0.9 mg/mL) was then dropcast onto the clean GC electrode surface by a Hamilton microliter syringe and was dried by a gentle nitrogen flow for ca. 2 min. The obtained electrodes were denoted as Ru/GC, PtRu/GC, and PtRu (BASF)/GC, respectively.

Voltammetric measurements were carried out with a CHI 440 electrochemical workstation. The Ru/GC, PtRu/GC, and PtRu (BASF)/GC electrodes prepared above were used as the working electrode. A Ag/AgCl wire and a Pt coil were used as the reference and counter electrodes, respectively. All electrode potentials in the present study were referred to this Ag/AgCl quasi-reference. Electrochemical impedance spectroscopy (EIS) measurements were carried out using an EG&G PARC Potentiostat/Galvanostat (model 283) and Frequency Response Detector (model 1025). The impedance spectra were recorded between 100 kHz and 10 mHz with the amplitude (rms value) of the ac signal 10 mV. The solutions were deaerated by bubbling ultra-high-purity N₂ for 20 min and protected with a nitrogen atmosphere during the entire experimental procedure.

2.4. Scanning tunneling microscopy and spectroscopy (STM/STS)

Thin films of Au(111) on mica, purchased from Molecular Imaging, were used as the substrates. Prior to use, the gold surfaces were cleaned with UV–ozone for 10 min (Model 42, Jelight Co.). The gold films were then immersed into a 1 mM solution of hexanedithiol in ethanol for 24 h for the formation of a self-assembled monolayer (SAM). The substrates were rinsed with excessive ethanol and blow-dried in a gentle stream of nitrogen. The dithiol modified Au(111) was then incubated into a RuSC8 particle solution for 24 h, followed by rinsing with ethanol and blow-drying with nitrogen. After being examined by STM and STS measurements with a PicoLE SPM instrument (from Molecular Imaging, operated at room temperature in air), the sample was immersed into a Pt(acac)₂ solution for 12 h before being rinsed by ethanol and

blow-dried with nitrogen again. The sample was then evaluated by STM and STS measurements. A mechanically cut Pt/Ir wire was used as the tip throughout the entire experiment. A high impedance of 75 M Ω (bias 1.5 V and set point 0.02 nA) was used to prevent tip damage or capture of the metal particles. STM topographic images were recorded in constant current mode. I - V data were collected in the spectroscopy mode where the feedback loop was turned off. At least 200 I - V data points were collected in a typical voltage sweep of ± 3 V. Every I - V curve was averaged for five times.

3. Results and discussion

Nanosized metal particles exhibit unique optical characteristics with an exponential decay of the absorption intensity with increasing wavelength (the so-called Mie scattering characteristics). Fig. 1 shows the UV-vis absorption spectra of the Ru nanoparticles before and after being immersed into a Pt(acac)₂ solution for 12 h. It can be seen that the Ru nanoparticles exhibit only a featureless absorption profile that is consistent with the Mie scattering behavior. However, for PtRu nanoparticles, there are two weak absorption peaks at 284 and 386 nm superimposed onto the exponential decay profile. These two peaks may be ascribed to the platinum complex adsorbed onto the Ru nanoparticle surface. Note that the particles had undergone extensive rinsing with acetone to remove excessive Pt(acac)₂. For comparison, the UV-vis spectrum of Pt(acac)₂ in dichloromethane is also included in Fig. 1, where two rather strong absorption peaks can be seen at around 294 and 352 nm. Of these, the higher energy band (294 nm) may be ascribed to the electronic transition of the diketone moieties of the acac ligands, whereas the lower energy band (352 nm) as a result of metal-ligand charge-transfer. Upon the binding of the complex onto the nanoparticle surface, the strong interaction between the Pt center and Ru electrons leads to a weakened metal-ligand (Pt-acac) bond. Consequently, the diketone band blue-shifts whereas the metal-ligand charge-transfer band red-shifts, as manifested above with the PtRu curve. The adsorbed Pt complex may then be reduced electrochemically and serve as active sites for electrocatalytic reactions (*vide infra*).

The adsorption of Pt(acac)₂ onto the Ru nanoparticle surface renders the particles more conductive, as manifested in scanning tunneling spectroscopic (STS) measurements. Fig. 2 shows a representative STM topographic image of Ru nanoparticles (a) before and (b) after Pt adsorption, which displays almost no difference in the diameter of the nanoparticles (around 4 nm). However,

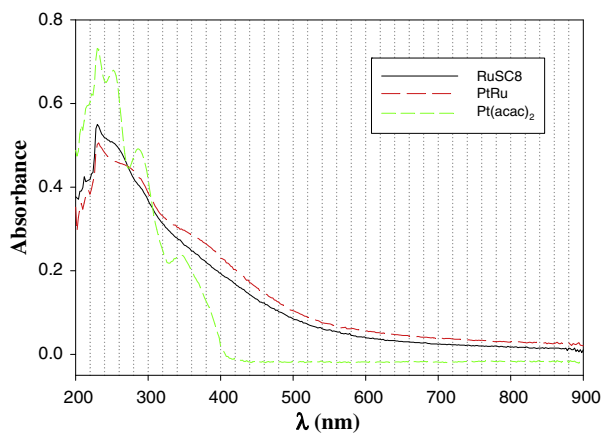


Fig. 1. UV-vis absorption spectra of the Ru nanoparticles before and after being immersed in a dichloromethane solution containing 1 mM Pt(acac)₂ for 12 h. Also shown is the absorption profile of the Pt(acac)₂ complex. Particle concentration are both 0.1 mg/mL in dichloromethane; whereas the Pt(acac)₂ concentration is 1 mM in dichloromethane.

results from STS measurements are drastically different. Panel (c) shows the I - V and dI/dV profiles of the original Ru nanoparticles, which exhibit a featureless flat region of about 1.1 V centered around the zero potential position, beyond which the Coulomb staircase features start to emerge. The appearance of a Coulomb blockade region is likely a consequence of the insulating alkane-thiolate protecting shells and the small particle core size. However, upon the adsorption of Pt(acac)₂ onto the Ru nanoparticles, the Coulomb blockade feature essentially vanishes (panel d), suggesting enhanced conductance of the nanoparticle molecules. Based on these STM and STS measurements, it is likely that the adsorbed Pt(acac)₂ complexes serve as the effective electron-tunneling sites to facilitate charge-transfer across the STM tip/particle/substrate junction.

Consistent results were obtained in voltammetric characterization of these two types of particles. Fig. 3 shows the cyclic voltammograms (CVs) of the Ru/GC, PtRu/GC, and PtRu (BASF)/GC electrodes in 0.1 M perchloric acid at a potential sweep rate of 0.1 V/s. No obvious voltammetric feature can be seen with the Ru/GC electrode, most probably because the blocking effect of the particle hydrophobic protecting layers renders the metal surface inaccessible by electrolyte ions. In contrast, after Pt(acac)₂ adsorption onto the Ru nanoparticle surface, several voltammetric features appear. First, in the potential range of -0.55 to -0.20 V, a pair of broad current peaks can be seen which correspond to the hydrogen adsorption and desorption on platinum surfaces. Second, the current density exhibits a drastic increase during the anodic and cathodic sweeps and there is a current peak around +0.1 V which may be attributed to the reduction of Pt oxide formed at more positive potentials during the positive sweep. It should be noted that the voltammetric features of the home-made PtRu nanoparticles are consistent with those of the commercial carbon-supported PtRu catalysts (though less pronounced), including the potential positions of hydrogen adsorption/desorption and the reduction of Pt oxide (+0.1 V). The appearance of a platinum voltammetric signature from PtRu/GC electrode strongly suggests that the adsorbed Pt(acac)₂ may be reduced into a thin Pt layer on the Ru particle surface. This observation is also consistent with the STM/STS results (Fig. 2) where the particles after Pt(acac) adsorption exhibit enhanced electrical conductance. Importantly, on the basis of the charge for the oxidation of surface-adsorbed hydrogen, the effective Pt surface area can be estimated to be 0.097 cm², by assuming that hydrogen desorption yields 210 $\mu\text{C cm}^{-2}$ of Pt surface area.

It should be noted that such an organic functionalization route based on monolayer-protected nanoparticles is in sharp contrast with that used previously in the spontaneous deposition of Pt onto Ru particles to prepare Ru@Pt near-surface-alloy particles. The latter was typically carried out with “naked” Ru nanoparticles in aqueous solutions of H₂PtCl₆ or H₂PtCl₄ under a reducing hydrogen or inert atmosphere [42–44].

In the electrocatalytic oxidation of methanol and formic acid, ruthenium is usually used as a second metal in Pt-based alloys to promote the deep oxidation of fuel molecules into CO₂. Here, the activity of the Ru, PtRu, and commercial PtRu nanoparticles in the electro-oxidation of formic acid was examined and compared by voltammetric and electrochemical impedance spectroscopy studies. Fig. 4 (black curve) shows the steady-state cyclic voltammograms of the Ru/GC electrode in 0.1 M HClO₄ and 0.1 M HCOOH at a potential scan rate of 0.1 V/s. There are two weak peaks at about +0.19 and +0.45 V in the anodic scan. As mentioned earlier, the electro-oxidation of methanol and formic acid typically follows a dual-pathway mechanism. That is, formic acid is either electro-oxidized directly to CO₂ by dehydrogenation or first dissociates spontaneously to CO which then becomes oxidized to CO₂. Thus, the anodic current peak at +0.19 V may be attributed to the

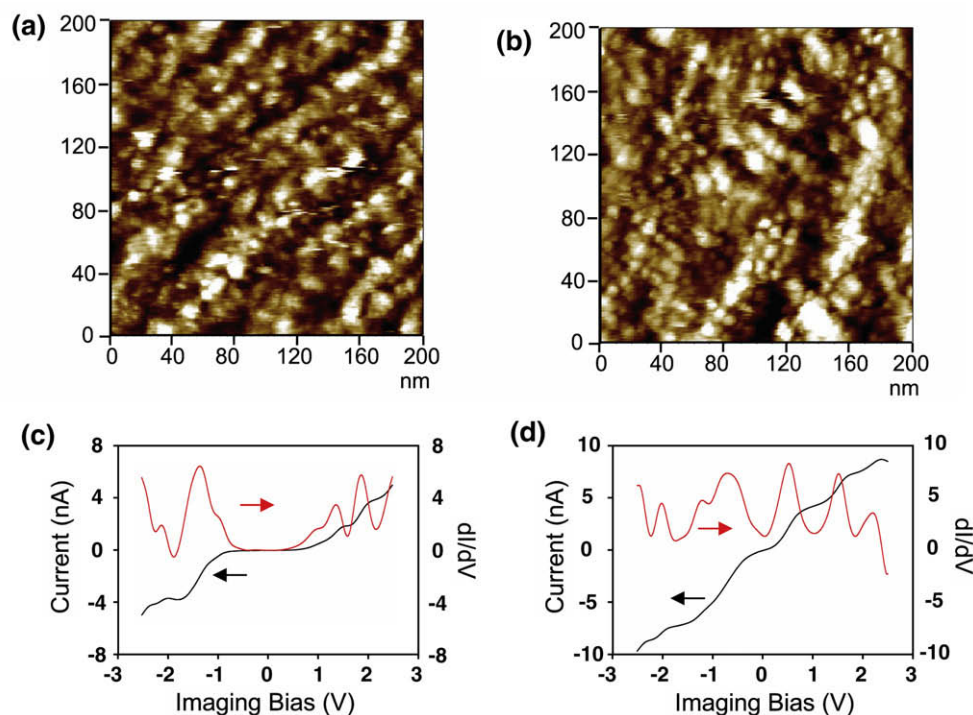


Fig. 2. STM topographs of the Ru nanoparticles (a) before and (b) after being immersed in a dichloromethane solution containing 1 mM Pt(acac)₂ for 12 h. The corresponding $I-V$ (black) and $dI/dV-V$ curves (red) are shown in panels (c) and (d), respectively. (For interpretation of the references to colour in this figure legend, the reader is referred to the web version of this article.)

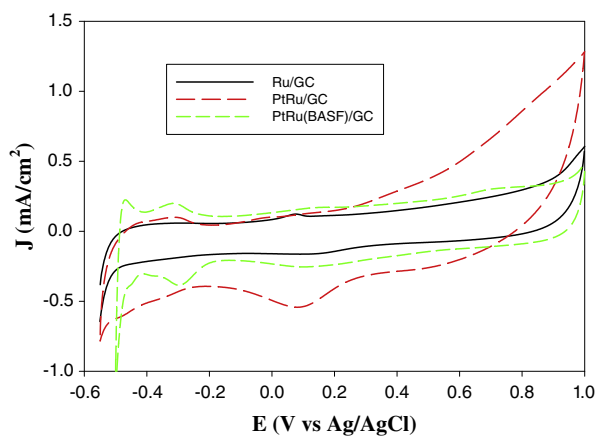


Fig. 3. Cyclic voltammograms of the Ru/GC (black curve), PtRu/GC (red curve) and PtRu (BASF)/GC (green curve) electrodes in 0.1 M HClO₄. The particle loadings were all 1.27 $\mu\text{g}/\text{mm}^2$. Potential scan rate 0.1 V/s. (For interpretation of the references to colour in this figure legend, the reader is referred to the web version of this article.)

oxidation of HCOOH on surface active sites that have not been poisoned by CO (direct path). The second anodic current peak at +0.45 V may arise from the oxidation of both adsorbed CO and formic acid as a consequence of the recovery of surface active sites by CO removal (indirect path). In the cathodic scan, a broad oxidation current peak at the potential of +0.22 V may be attributed to the oxidation of formic acid through the active intermediate. Yet, the overall low current density suggests that ruthenium is catalytically inefficient in the oxidation of formic acid, similar to earlier studies in the electro-oxidation of methanol at a ruthenium thin film electrode deposited on a Au electrode [48].

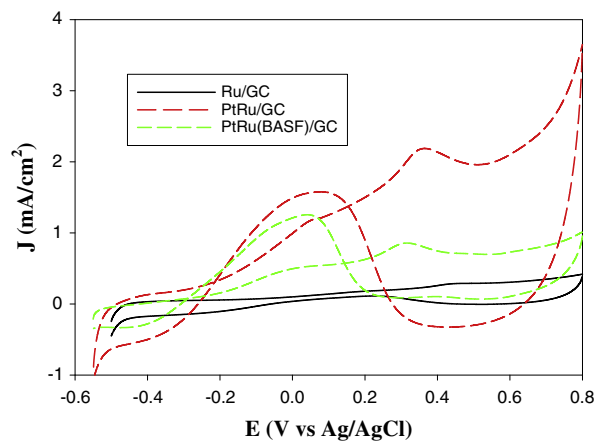


Fig. 4. Steady-state cyclic voltammograms of Ru/GC (black curve), PtRu/GC (red curve) and PtRu (BASF)/GC (green curve) electrodes in 0.1 M HCOOH and 0.1 M HClO₄. The particle loadings were all 1.27 $\mu\text{g}/\text{mm}^2$. Potential scan rate 0.1 V/s. (For interpretation of the references to colour in this figure legend, the reader is referred to the web version of this article.)

In sharp contrast, upon Pt deposition onto the Ru surface, the electrocatalytic activity improves drastically. Fig. 4 (red curve¹) shows the cyclic voltammogram of formic acid oxidation at the PtRu/GC electrode. First, it can be seen that the current density is enhanced by at least an order of magnitude, as compared to that of the Ru/GC electrode (black curve). Second, in the anodic sweep, there are two oxidation peaks at +0.075 V and +0.364 V, which correspond to the direct oxidation of HCOOH and the oxidation of adsorbed CO and HCOOH, respectively. Note that the potential positions of these two

¹ Please note that Figs. 2–4 will appear in B/W in print and color in the web version. Based on this, please approve the footnote 1 which explains this.

peaks are somewhat more negative than those at the Ru/GC electrode (vide ante). In addition, it can be seen that the onset potential also shows a cathodic shift of 0.2 V from ca. -0.2 V (Ru/GC) to -0.4 V (PtRu/GC). These results indicate that the deposition of a Pt thin-layer led to significant improvement of the catalytic activity in the electro-oxidation of formic acid. This may be attributed to the unique characteristics of Ru to adsorb oxygen-containing species that are essential in the oxidation of CO adsorbed on nearby Pt sites. Additionally, one can see that the current density of HCOOH oxidation at the PtRu/GC electrode is higher than that obtained from commercial PtRu particles (green curve), although the peak potential on PtRu/GC ($+0.36$ V) is slightly more positive than that at PtRu (BASF)/GC ($+0.31$ V).

Further comparison can be made by the ratio of the current density of the first anodic peak (J_a) to the cathodic peak (J_c), which has been used to evaluate the catalyst tolerance to CO poisoning. From Fig. 4, the J_a/J_c ratio on PtRu/GC is ca. 0.84, whereas on PtRu (BASF)/GC, 0.52, suggesting enhanced CO tolerance of the homemade PtRu nanoparticles as compared to the commercial ones.

It should be noted that in the above measurements of homemade PtRu nanoparticles, no special procedure was employed to remove the alkanethiolate protecting layer. Thus, it was somewhat surprising and yet remarkable to observe obvious electrocatalytic activity in the oxidation of HCOOH at PtRu/GC. One plausible explanation is that the deposition of Pt onto the Ru particles led to at least partial desorption of the thiolate ligands, which rendered the nanoparticle surface accessible by fuel molecules. By using monolayer-passivated nanoparticles as the starting materials, it becomes possible to control the particle size and structural uniformity in an unprecedented degree of accuracy, because of the well-established synthetic protocols and detailed structural characterization procedures. This remains a challenge in conventional colloidal systems. Certainly, at the moment, the exact content of the organic protecting ligands in the nanoparticle catalysts and their impacts on the electrocatalytic performance remain unknown. These issues will be examined in ongoing work.

Furthermore, comparison to other Pt-based alloy particles shows that despite the minimal loading of Pt onto the Ru particle surface, the electrocatalytic activity of the PtRu particles is highly comparable. For instance, the onset potential at the PtRu/GC electrode is almost the same as that at the $\text{Fe}_{42}\text{Pt}_{58}$ nanoparticles (-0.4 V vs. Ag/AgCl), which ranks the best among the series of $\text{Fe}_x\text{Pt}_{100-x}$ alloy nanoparticles ($x = 10\text{--}65$) in the electro-oxidation of HCOOH [19]. However, the current density at the PtRu/GC electrode is about two orders of magnitude lower than that at the $\text{Fe}_{42}\text{Pt}_{58}$ /GC counterpart [19], but significantly larger than that of methanol oxidation at polycrystalline PtRu bulk alloys [49]. This may be attributable to the incomplete removal of the hydrophobic alkanethiolate protecting shell which hampers the access of fuel molecules to the electrode surface. Obviously, optimization of the catalyst structures and loading is needed to further improve the catalytic performance.

The electron-transfer kinetics of formic acid oxidation was further examined by electrochemical impedance spectroscopy measurements. Overall the impedance profiles are very consistent with the voltammetric results. Importantly, by comparing the Nyquist plots of formic acid oxidation at the Ru/GC, PtRu/GC, and PtRu (BASF)/GC electrodes (Fig. 5), it can be seen that the diameter of the impedance arcs at the PtRu/GC electrode is at least one order of magnitude smaller than that at the Ru/GC and PtRu (BASF)/GC counterparts, suggestive of substantially lower charge-transfer resistance and higher catalytic activity of the PtRu nanoparticles.

For the Ru/GC electrode (panel a), it can be seen that at 0.0 V, the impedance shows a large arc in the first quadrant, which indicates the presence of resistive and capacitive components and a slow electron-transfer rate of formic acid oxidation. With increas-

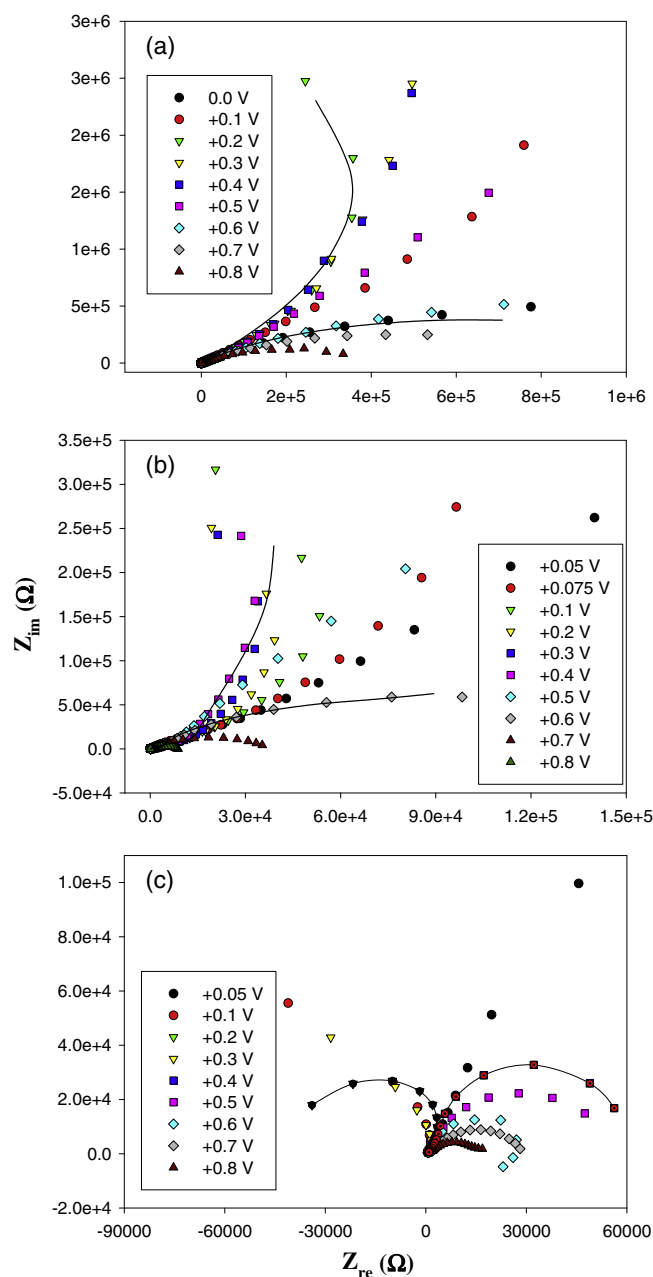


Fig. 5. Nyquist plots of (a) Ru/GC, (b) PtRu/GC, and (c) PtRu (BASF)/GC electrodes in 0.1 M HCOOH and 0.1 M HClO₄. The particle loadings were all 1.27 $\mu\text{g}/\text{mm}^2$. The electrode potentials are shown as figure legends. Solid lines are representative simulations based on the equivalent circuits shown in Fig. 6 insets.

ing potential, the arc bends from the positive to negative direction of the x axis. This impedance feature has also been encountered in formic acid oxidation on FePt particles [19,20,50], and ascribed to the oxidation of adsorbed CO intermediate and the recovery of the catalytic sites. In the voltammetric measurements (Fig. 4), it can be seen that between the potentials of $+0.1$ and $+0.4$ V, adsorbed CO is oxidized, leading to enhanced activity of the electrode for HCOOH oxidation. With a further increase of the electrode potential ($>+0.5$ V), the impedance plots return to normal behaviors (bending to the positive direction of the x axis) and concurrently the diameter of the arc decreases.

At the PtRu/GC electrode (panel b), one can see that at potentials more positive than $+0.05$ V, the arc starts to bend from the positive to negative direction of the x axis and the diameter decreases

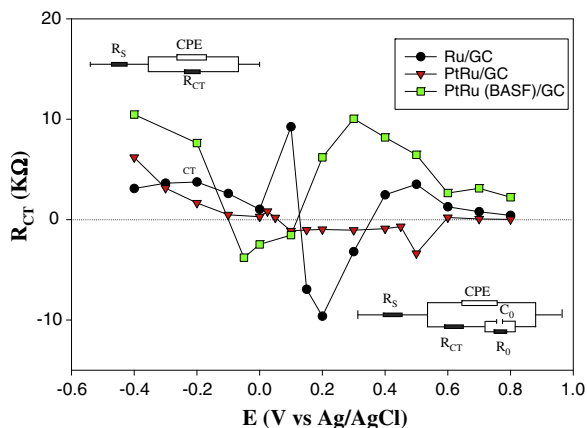


Fig. 6. Variation of charge-transfer resistance (R_{CT}) with electrode potentials for the Ru/GC, PtRu/GC, and PtRu (BASF)/GC electrodes in 0.1 M HCOOH and 0.1 M HClO₄. Data were obtained from fitting of the Nyquist plots of the electrochemical impedance spectra (Fig. 5) by the equivalent circuits (insets). The top inset represents the equivalent circuit for normal impedance, where R_s is the solution resistance, CPE (constant-phase element) the double layer capacitance, and R_{CT} charge-transfer resistance. The bottom inset is the equivalent circuit for negative impedance, where C_0 and R_0 represent the capacitance and resistance of the electro-oxidation of adsorbed CO intermediates.

with increasing potential, also in good agreement with the voltammetric results (Fig. 4). And again, the impedance plots return to normal behaviors at potentials more positive than +0.5 V and the diameter of the arc decreases quickly with increasing potential.

Fig. 5c depicts the impedance spectra of HCOOH oxidation at PtRu (BASF)/GC electrode at different potentials. It can be seen that, at the potential of +0.05 V, the impedance arc is located within the first quadrant. However, at potentials from +0.1 to +0.3 V, negative Faradaic impedance can be observed in the second quadrant, which is different from the impedance spectra of Ru/C and PtRu/C (Fig. 5a and b). The negative impedance suggests that rather extensive CO oxidation occurred at the PtRu (BASF)/GC electrode, in good agreement with the voltammetric results where rather heavy CO poisoning was observed on commercial PtRu particles (Fig. 4).

Based on the voltammetric and impedance results, the equivalent circuits shown as insets to Fig. 6 were used to fit the impedance data on Ru/GC, PtRu/GC, and PtRu (BASF)/GC electrodes. The top inset depicts the equivalent circuit for the electrodes that exhibit normal impedance behaviors, where R_s represents the solution resistance, CPE (constant-phase element) and R_{CT} are the double layer capacitance and charge-transfer resistance, respectively. For negative impedance, the equivalent circuit is shown in the bottom inset, where C_0 and R_0 represent the capacitance and resistance of the electro-oxidation of adsorbed CO intermediates. Several representative fits (solid lines) for the three electrodes were shown in the Nyquist plots in Fig. 5, all of which show good agreement with the experimental data.

The overall variation of the charge-transfer resistance (R_{CT} , obtained by fitting the impedance spectra with an appropriate equivalent circuit) with electrode potentials was depicted in Fig. 6. It can be seen that within the potential range of -0.4 V to +0.8 V, R_{CT} is indeed markedly smaller at the PtRu/GC electrode than at the Ru/GC and PtRu (BASF)/GC electrodes. Yet, the overall changing trend is similar for these three electrodes. That is, at low potentials (<0 V), R_{CT} decreases rapidly with increasing electrode potential; within the potential range where the oxidative removal of adsorbed CO occurs, R_{CT} reverses from positive to negative values, signifying the emergence of an inductive component; and at higher electrode potentials, R_{CT} decreases again with increasing potential. The behaviors are consistent with the

voltammetric results (Fig. 4). Taken together, these results suggest significant enhancement of the catalytic performance by the decoration of a platinum thin-layer on the ruthenium nanoparticle surface, which even exceeds that of a commercial PtRu particle catalyst.

4. Conclusions

Spontaneous adsorption of Pt(acac)₂ onto ruthenium nanoparticles occurred despite the coating of a hydrophobic alkanethiolate protecting layer on the particle surface. The adsorption was suspected to arise from the strong affinity of the platinum metal center to the ruthenium surface. Electrochemical reduction led to the deposition of Pt onto the ruthenium particle surface, and hence the formation of PtRu surface-alloy particles. The catalytic activity of the resulting nanoparticles in the electro-oxidation of formic acid was then evaluated and compared. Both voltammetric and electrochemical impedance measurements showed that the deposition of a minimal amount of Pt onto the Ru nanoparticle surface led to drastic improvement of the electrocatalytic activity, in comparison to the original Ru nanoparticles and commercial PtRu nanoparticle catalysts, which had been manifested by the cathodic shift of the onset potential for the electro-oxidative removal of poisonous intermediate CO that was adsorbed onto the catalyst surface as well as by the variation of the charge-transfer resistance with electrode potentials. The catalytic activity of the PtRu particles was also found to be comparable to that of other platinum-based alloys that had been commonly used in the electro-oxidation of small fuel molecules, demonstrating the fundamental significance of surface engineering in the improvement and optimization of nanoparticle catalysts in fuel cell electrochemistry.

It should be noted that in the present study no particular procedure was employed to remove the organic protecting ligands, largely to keep the particle structure and size unchanged during the electrochemical measurements. Yet the well-defined voltammetric features for platinum (Fig. 3) strongly suggest that the nanoparticle surface was highly accessible. This is further manifested in the subsequent measurements of formic acid electro-oxidation (Fig. 4) where apparent enhancement of the current density as well as CO tolerance was observed as compared to commercial PtRu nanoparticles. Further work is being carried out to examine the structural details of the nanoparticle catalysts and their effects on the electrocatalytic performance.

Acknowledgment

This work was supported by the National Science Foundation (CHE-0718190 and DMR-0804049).

References

- [1] S.C. Thomas, X.M. Ren, S. Gottesfeld, P. Zelenay, *Electrochimica Acta* 47 (2002) 3741.
- [2] X.M. Ren, P. Zelenay, S. Thomas, J. Davey, S. Gottesfeld, *Journal of Power Sources* 86 (2000) 111.
- [3] S. Wasmus, A. Kuver, *Journal of Electroanalytical Chemistry* 461 (1999) 14.
- [4] Y.M. Zhu, Z. Khan, R.I. Masel, *Journal of Power Sources* 139 (2005) 15.
- [5] G.Q. Lu, A. Crown, A. Wieckowski, *Journal of Physical Chemistry B* 103 (1999) 9700.
- [6] W.P. Zhou, A. Lewera, R. Larsen, R.I. Masel, P.S. Bagus, A. Wieckowski, *Journal of Physical Chemistry B* 110 (2006) 13393.
- [7] H. Abe, F. Matsumoto, L.R. Alden, S.C. Warren, H.D. Abruna, F.J. DiSalvo, *Journal of the American Chemical Society* 130 (2008) 5452.
- [8] E. Casado-Rivera, D.J. Volpe, L. Alden, C. Lind, C. Downie, T. Vazquez-Alvarez, A.C.D. Angelo, F.J. DiSalvo, H.D. Abruna, *Journal of the American Chemical Society* 126 (2004) 4043.
- [9] W.F. Lin, M.S. Zei, M. Eiswirth, G. Ertl, T. Iwasita, W. Vielstich, *Journal of Physical Chemistry B* 103 (1999) 6968.
- [10] T. Frelink, W. Visscher, J.A.R. vanVeen, *Langmuir* 12 (1996) 3702.
- [11] K.W. Park, J.H. Choi, B.K. Kwon, S.A. Lee, Y.E. Sung, H.Y. Ha, S.A. Hong, H. Kim, A. Wieckowski, *Journal of Physical Chemistry B* 106 (2002) 1869.

- [12] F. Colmati, E. Antolini, E.R. Gonzalez, *Electrochimica Acta* 50 (2005) 5496.
- [13] T. Page, R. Johnson, J. Hormes, S. Noding, B. Rambabu, *Journal of Electroanalytical Chemistry* 485 (2000) 34.
- [14] S. Motoo, M. Watanabe, *Journal of Electroanalytical Chemistry* 69 (1976) 429.
- [15] J.Y. Lee, P. Strasser, M. Eiswirth, G. Ertl, *Electrochimica Acta* 47 (2001) 501.
- [16] R.S. Jayashree, J.S. Spendelow, J. Yeom, C. Rastogi, M.A. Shannon, P.J.A. Kenis, *Electrochimica Acta* 50 (2005) 4674.
- [17] L.B. Lai, D.H. Chen, T.C. Huang, *Journal of Materials Chemistry* 11 (2001) 1491.
- [18] H. Yang, N. Alonso-Vante, J.M. Leger, C. Lamy, *Journal of Physical Chemistry B* 108 (2004) 1938.
- [19] W. Chen, J.M. Kim, S.H. Sun, S.W. Chen, *Langmuir* 23 (2007) 11303.
- [20] W. Chen, J.M. Kim, L.P. Xu, S.H. Sun, S.W. Chen, *Journal of Physical Chemistry C* 111 (2007) 13452.
- [21] T. Frelink, W. Visscher, A.P. Cox, J.A.R. Vanveen, *Electrochimica Acta* 40 (1995) 1537.
- [22] K.L. Ley, R.X. Liu, C. Pu, Q.B. Fan, N. Leyarovska, C. Segre, E.S. Smotkin, *Journal of the Electrochemical Society* 144 (1997) 1543.
- [23] J.J. Wu, J.B. Day, K. Franaszczuk, B. Montez, E. Oldfield, A. Wieckowski, P.A. Vuissoz, J.P. Ansermet, *Journal of the Chemical Society–Faraday Transactions* 93 (1997) 1017.
- [24] E. Spinace, A.O. Neto, M. Linardi, *Journal of Power Sources* 129 (2004) 121.
- [25] B. Yang, Q.Y. Lu, Y. Wang, L. Zhuang, J.T. Lu, P.F. Liu, *Chemistry of Materials* 15 (2003) 3552.
- [26] E.S. Steigerwalt, G.A. Deluga, C.M. Lukehart, *Journal of Physical Chemistry B* 106 (2002) 760.
- [27] C.W. Hills, N.H. Mack, R.G. Nuzzo, *Journal of Physical Chemistry B* 107 (2003) 2626.
- [28] J.L.G. de la Fuente, M.V. Martinez-Huerta, S. Rojas, P. Terreros, J.L.G. Fierro, M.A. Pena, *Catalysis Today* 116 (2006) 422.
- [29] M. Watanabe, M. Uchida, S. Motoo, *Journal of Electroanalytical Chemistry* 229 (1987) 395.
- [30] D.L. Boxall, J.J. O’Dea, R.A. Osteryoung, *Journal of the Electrochemical Society* 149 (2002) E468.
- [31] Y.M. Liang, H.M. Zhang, H.X. Zhong, X.B. Zhu, Z.Q. Tian, D.Y. Xu, B.L. Yi, *Journal of Catalysis* 238 (2006) 468.
- [32] F. Bensebaa, N. Patrito, Y. Le Page, P. L’Ecuyer, D.S. Wang, *Journal of Materials Chemistry* 14 (2004) 3378.
- [33] Z.G. Shao, F.Y. Zhu, W.F. Lin, P.A. Christensen, H.M. Zhang, *Physical Chemistry Chemical Physics* 8 (2006) 2720.
- [34] A. Missiroli, F. Soavi, M. Mastragostino, *Electrochemical and Solid State Letters* 8 (2005) A110.
- [35] V. Del Colle, A. Berna, G. Tremiliosi, E. Herrero, J.M. Feliu, *Physical Chemistry Chemical Physics* 10 (2008) 3766.
- [36] Z.L. Liu, J.Y. Lee, M. Han, W.X. Chen, L.M. Gan, *Journal of Materials Chemistry* 12 (2002) 2453.
- [37] J.L. Zhang, M.B. Vukmirovic, Y. Xu, M. Mavrikakis, R.R. Adzic, *Angewandte Chemie-International Edition* 44 (2005) 2132.
- [38] J. Greeley, M. Mavrikakis, *Catalysis Today* 111 (2006) 52.
- [39] S. Alayoglu, A.U. Nilekar, M. Mavrikakis, B. Eichhorn, *Nature Materials* 7 (2008) 333.
- [40] J.A. Rodriguez, *Surface Science Reports* 24 (1996) 225.
- [41] M. Arenz, V. Stamenkovic, P.N. Ross, N.M. Markovic, *Surface Science* 573 (2004) 57.
- [42] S.T. Kuk, A. Wieckowski, *Journal of Power Sources* 141 (2005) 1.
- [43] J.X. Wang, S.R. Brankovic, Y. Zhu, J.C. Hanson, R.R. Adzic, *Journal of the Electrochemical Society* 150 (2003) A1108.
- [44] S.R. Brankovic, J.X. Wang, R.R. Adzic, *Electrochemical and Solid-State Letters* 4 (2001) A217.
- [45] N. Chakroune, G. Viau, S. Ammar, L. Poul, D. Veautier, M.M. Chehimi, C. Mangeney, F. Villain, F. Fievet, *Langmuir* 21 (2005) 6788.
- [46] G. Viau, R. Brayner, L. Poul, N. Chakroune, E. Lacaze, F. Fievet-Vincent, F. Fievet, *Chemistry of Materials* 15 (2003) 486.
- [47] W. Chen, J.R. Davies, D. Ghosh, M.C. Tong, J.P. Konopelski, S.W. Chen, *Chemistry of Materials* 18 (2006) 5253.
- [48] H.Z. Yang, Y.Q. Yang, S.Z. Zou, *Journal of Physical Chemistry B* 110 (2006) 17296.
- [49] H.A. Gasteiger, N. Markovic, P.N. Ross, E.J. Cairns, *Journal of Physical Chemistry* 97 (1993) 12020.
- [50] W. Chen, J. Kim, S.H. Sun, S.W. Chen, *Physical Chemistry Chemical Physics* 8 (2006) 2779.